Mode-locked 1.5 micrometers semiconductor optical amplifier fiber ring

Pedersen, Niels V.; Jakobsen, Kaj Bjarne; Vaa, Michael

Published in:
Journal of Lightwave Technology

Link to article, DOI:
10.1109/50.495165

Publication date:
1996

Document Version
Publisher's PDF, also known as Version of record

Mode-Locked 1.5 μm Semiconductor Optical Amplifier Fiber Ring

Niels V. Pedersen, Kaj B. Jakobsen, and Michael Vaa

Abstract—**The dynamics of a mode-locked SOA fiber ring are investigated experimentally and numerically. Generation of near transform-limited (time-bandwidth product = 0.7) 1.5 μm 54 ps FWHM pulses with a peak power of 2.8 mW at a repetition rate of 960 MHz is demonstrated experimentally. The experimental results agree well with the simulation results obtained using a TLLM model. Both experiments and numerical simulations show how the RF power and the detuning affect the pulsewidth.**

I. Introduction

SEMICONDUCTOR components are attractive as compact sources for generation of short optical pulses at high repetition rates for use, e.g., in OTDM transmission systems. Pulse generation using mode-locked linear external cavity semiconductor lasers is a well-known technique, which gives excellent results as described, e.g., in [1], [2]. This work considers a different approach based on a semiconductor optical amplifier (SOA) inserted into a fiber ring. Such ring lasers are not extensively described in literature, and the influence on the generated pulses originating from features characteristic of the ring geometry is therefore not thoroughly investigated.

One of the main features of semiconductor components is the possibility of monolithic integration and lately mode-locking of monolithical ring lasers has been demonstrated [3], [4] but though offering the advantage of complete monolithic integration these devices are inherently associated with very high resonance frequencies (>9 GHz) that limit the repetition rate downwards.

In this paper the dynamics of a mode-locked SOA ring laser are characterized. A mode-locked pulse train is obtained by modulating the current to a SOA inserted into an optical fiber ring. The modulation frequency can be either the fundamental resonance frequency of the ring or a higher harmonic.

The experimental results are compared with numerical simulations in order to determine the factors that influence the pulse envelope. The numerical simulations are performed using a transmission-line laser model (TLLM) [5], [6].

In Section II, the theoretical background is described. Section III gives an overview of the TLLM model used in the simulations. Section IV presents the results and finally, Section V gives a discussion of the results and conclusions of this paper.

Manuscript received September 3, 1993; revised January 23, 1995.

The authors are with the Center for Broadband Telecommunications, Electromagnetics Institute, Technical University of Denmark, DK-2800 Lyngby, Denmark.

Publisher Item Identifier S 0733-8724(96)03885-6.

II. Theory

Here, we consider active mode-locking using gain modulation. Modulation of the SOA bias current leads to generation of a comb spectrum where all the sidebands are in phase and a corresponding comb shaped signal in the time domain—a pulse train. The pulse train will have a repetition frequency equal to the modulation frequency. Assuming a constant round-trip gain $\alpha_m p_m$, the resulting FWHM steady-state pulsewidth $\tau_{p,ss}$ is derived in [1] as

$$\tau_{p,ss} = \sqrt{\frac{2\sqrt{2}\cdot \ln 2}{\pi^2}} \cdot \sqrt[4]{\frac{\alpha_m p_m}{\Delta_m}} \cdot \sqrt{\frac{1}{f_{\mathrm{MOD}} \Delta f_a}} \quad (1)$$

where Δ_m is the modulation index, $\alpha_m p_m$ is the round-trip voltage gain coefficient, f_{MOD} is the modulation frequency, and Δf_a is the atomic linewidth of the semiconductor material. The steady state pulsewidth is defined as the width when the change in pulse envelope between two subsequent round-trips is zero.

Equation (1) argues that when a steady state is reached the pulsewidth $\tau_{p,ss}$ is fully determined by a rather small number of parameters. For example, a simple $(f_{\mathrm{MOD}})^{-1/2}$ dependence should be expected. However, in addition to the parameters included in Equation (1) there are a few other well-known phenomena that affect the final pulse envelope, namely, the pulse shaping due to gain saturation and fiber nonlinearities. The round-trip gain may vary somewhat due to carrier depletion in the active region of the SOA. When a pulse propagates through the SOA the high intensity causes a depletion of the carriers. As a result the gain will saturate and the envelope of the output pulse will change. Depending on the intensity of the input pulse, gain saturation can result in either a narrowing or broadening of the output pulse. Narrowing of the pulse is seen if the gain saturates on the trailing edge of the input pulse, which causes a part of the edge to be "cut" off. If the intensity of the input pulse is very high, however, the gain saturates on the leading edge causing the pulse envelope to be broadened. This indicates that carrier depletion is an important factor in the forming of the steady state pulse envelope. The nonlinearities in the optical fiber also give rise to pulse shaping but this effect is of minor significance in the setup considered here, and is therefore not included in our simulations.

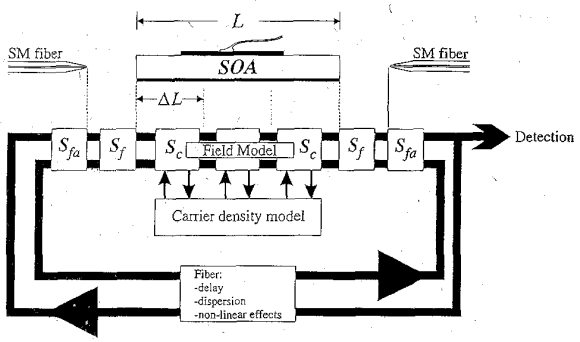

Fig. 1. Schematic representation of the TLLM model. The SOA cavity is divided into three sections with corresponding scattering matrices S_c. SOA facets and fiber ends are modeled with scattering matrices S_f and S_{fa}, respectively.

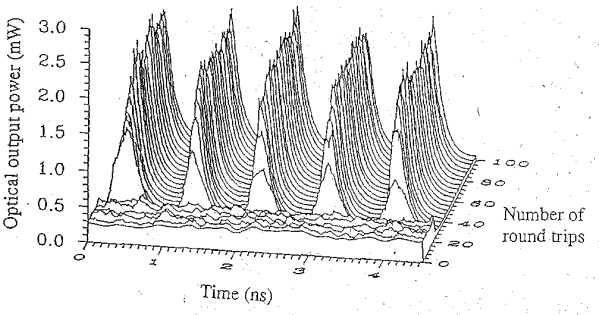

Fig. 2. Simulated dynamic evolution of a mode-locked pulse train. The ring laser is modulated at the fifth harmonic resulting in five independent circulating pulses in the ring. It is seen that a stable pulse train has evolved after only a few round trips.

It is important to note, that the described characteristics of mode-locking apply to linear cavity lasers as well as to the ring geometry. However, as linear cavity lasers in general have shorter cavity lengths compared to the ring configuration discussed here, the aspects of mode-locking at a high harmonic of the cavity resonance frequency have been subject to little investigation.

III. Simulation

The pulse train generation and evolution in the ring laser has been simulated using a transmission-line laser model that is well described in literature [5], [7], [8], but until now used in association with linear external cavity lasers only. In this work the TLLM model is used for the first time to model a ring laser. A schematic representation of the TLLM model is shown in Fig. 1. The SOA of length L is divided spatially into a number of sections s_0 with equal length ΔL—in this example three sections. In the model the optical bandwidth of the device is simply limited via the Nyquist limitation by the number of sections, the number of modeled longitudinal modes being equal to s_0. In each section a field model and a carrier density model are operated simultaneously. The optical field and the carrier density are modeled as voltages on the transmission lines and interconnected by the laser rate equations. In the field model the optical processes within each section are described by a scattering matrix $\boldsymbol{S}_c$ including models for the spontaneous and stimulated emission and attenuation of the optical field. $\boldsymbol{S}_c$ is fully described by Lowery, e.g., in [5], [7]. The SOA facets are described by scattering matrices $\boldsymbol{S}_f$ which include chip reflections due to residual reflectivity, coupling to external fields and chirp. Coupling loss and reflections at the fiber ends are described by scattering matrices $\boldsymbol{S}_{fa}$. The carrier density model for each section also includes all optical processes plus carrier diffusion along the active region of the SOA. The main feature of the TLLM model is that it models the optical field and not the intensity. Therefore the phase information of the signal is available which has been shown to be crucial for correct modeling, e.g., of reflections at the facets of the amplifier [5].

All scattering matrices are connected with transmission lines. These have a length which has been chosen so the reflected field from one section during one time step becomes the incident field to the next section during the next time step. This is done simply by choosing the time step ΔT equal to the field propagation time for one section, i.e.

$$\Delta T = \frac{\Delta L \overline{n}_e}{c} \tag{2}$$

where $\overline{n}_e$ is the cavity group index of refraction and c is the velocity of light in vacuum. The fiber ring is modeled by a simple FIFO delay line which can be combined with a scattering matrix in each fiber section to include e.g. dispersion effects. A dispersion model of an optical fiber has been developed, but it is assumed that dispersion has very little effect on the generated pulses as the fiber length is relatively short. Therefore, the dispersion model is not included in the work presented here in order to save CPU time. Due to the large fiber round trip delay associated with the ring geometry considered here (approximately 60 ns) compared to the small delay found for most linear external cavity lasers (in the order of 0.4–0.5 ns) calculation time has to be considered carefully. As a result, the number of SOA sections has been reduced from around 100–200 [7], [8] to 8 (for a 500 μm long SOA). According to [7] this leads to a decreased model gain accuracy, but simulations show that good results can be obtained with fewer sections by decreasing the field attenuation accordingly.

Fig. 2 shows a TLLM simulation of the evolution of a mode-locked pulse train in the ring laser. Here, the length of the external cavity is 1.0 m and every fourth round trip is shown. The SOA is modulated at the fifth harmonic and therefore five independent pulses circulate in the ring. Modulation starts after 20 round-trips. Note that after only another 30–40 round-trips a stable pulse train has evolved. This is in excellent agreement with earlier results obtained using the TLLM model [9]. Other models, however (e.g., [10]–[12]), have shown that it requires several hundred round-trips for the pulse train to stabilise. The reason for the fast convergence seen in the TLLM model is not fully understood, but may be due to the fact that several longitudinal modes are modeled in contrast to [11] where only a single oscillating mode is considered. Simulations also indicate that the time needed for the pulse train to stabilise decreases with increasing number of the harmonic of the cavity resonance frequency at which the SOA is modulated. This is likely to be caused by the external cavity

TABLE I
MATERIAL PARAMETERS USED IN THE SIMULATIONS

Parameter	Symbol	Value
Effective group index of refraction in cavity	$\bar{n}_e$	3.7
Differential gain, $dg(peak)/dN$	a_1	$2.7\cdot10^{-16}$ cm^2
Parabola width parameter	a_2	$4.0\cdot10^{5}$ eV$^{-2}\cdot$cm^{-1}
Shift in peak gain energy, dE_g/dN	a_3	$1.4\cdot10^{-20}$ eV$\cdot$cm^3
SOA confinement factor	Γ_{SOA}	0.3
Transparency carrier density	N_0	$0.9\cdot10^{18}$ cm^{-3}
Carrier lifetime	τ_s	$1.7\cdot10^{-9}$ s
Width of active region	w	$5\cdot10^{-6}$ m
Height of active region	d	$0.15\cdot10^{-6}$ m
Length of SOA	L	$500\cdot10^{-6}$ m
Length of external cavity	L_R	1.0 m
Linewidth enhancement factor	α	5.6
SOA attenuation per unit length	α_{sc}	$40.0\cdot10^{2}$ m^{-1}
Free space gain peak wavelength	λ_0	$1520\cdot10^{-9}$ m
Number of SOA model sections	s_0	8
Spontaneous emission coupling factor	β	$1.0\cdot10^{-5}$
PIN diode time constant	τ_{PIN}	$25\cdot10^{-12}$ s

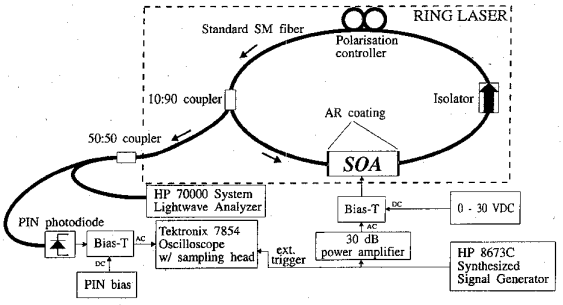

Fig. 3. Experimental setup. The SOA is placed in a fiber ring including a polarization controller and an optical isolator. Shown are also the SOA bias circuit and the instruments used for detection of the mode-locked signal.

modes coupling easier to the RF signal when the latter contains larger frequency components at the higher harmonics.

The simulations were performed on an IBM RISC-SYSTEM/6000 work station. The calculation time is approximately 12 h using eight chip-sections and a fiber loop of length 11.8 m. The model parameters used in the simulations are given in Table I.

IV. RESULTS

The experimental setup of the SOA ring laser is shown in Fig. 3. An optical isolator and a polarization controller are inserted into the fiber ring to ensure maximum power circulating in one direction. The polarization has been adjusted for maximum circulating power. An optical 10:90-coupler is placed in the ring cavity for coupling out the signal.

In the experiments two structural different SOA's have been used. SOA #1 is a buried heterostructure device with a length of 500 μm and it is AR-coated to approximately $2\cdot10^{-2}$ on both facets. The active region is angled 7° with respect to the facets. The lasing threshold is 42 mA for the chip itself and 26 mA for the ring laser. The ring is lasing at 1523 nm in one polarization only. SOA #2 is a ridge waveguide structure with a length of 500 μm and it is AR-coated to 10^{-4} – 10^{-5}. The active region is angled 10° with respect to the facets. Due to the very low facet reflectivity no lasing threshold was observed for the chip itself. The threshold for the ring laser is 75 mA. The lasing wavelength is 1550 nm or 1561 nm depending on the state of polarization. The fiber used in the setup is

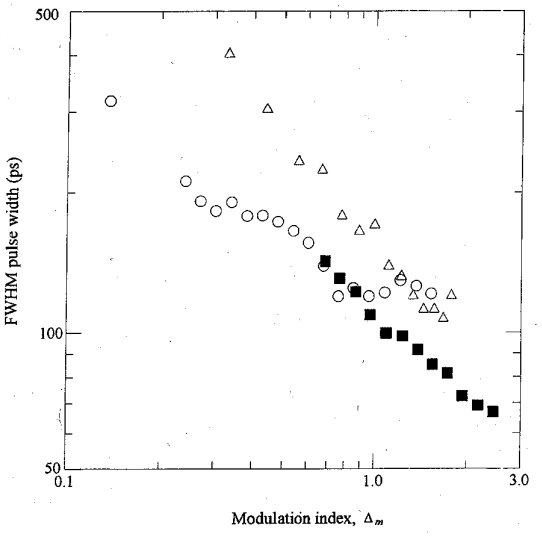

Fig. 4. Measured (SOA #1 (■) and SOA #2 (○)) and simulated (△) deconvolved FWHM pulsewidth as a function of the modulation index.

standard SM fiber. The signal is coupled to and from the SOA using AR-coated tapered lens ended fibers. Both SOA's are DC-biased at the lasing threshold for the ring laser.

Fig. 4 shows the deconvolved FWHM pulsewidth versus the modulation index Δ_m. Both the measured and simulated results are shown. Note, that due to the fact that the modeling of a PIN photo diode is included in the TLLM model, the simulated pulsewidths must be deconvolved with respect to the photo diode time constant, also. From (1) the FWHM pulsewidth is expected to decrease with increasing RF power as $\tau_{p,ss} \propto (\Delta_m)^{-1/4}$. From the measurements shown in Fig. 4 it is clear however, that the slope is not -0.25, but -0.60 and -0.37 for SOA #1 and SOA #2, respectively. Likewise, simulations show a slope of -0.78. The deviation from the theoretically expected can be explained by the large detuning, $\Delta_f = f_{\mathrm{MOD}} - f_{\mathrm{crf}}$ of the modulation frequency f_{MOD} away from the cavity resonance frequency f_{crf} needed to obtain optimum performance. Large detuning (i.e., $\Delta_f > 0.5\%$) is shown [8], [11] to obstruct the evolution of a steady-state pulse train as defined in [1] and even to cause instabilities. Therefore, in the case of $f_{\mathrm{MOD}} \neq f_{\mathrm{crf}}$, the pulse envelope should rather be considered as being in a continuously dynamic state of equilibrium referred to by Morton et al. [13] as dynamic detuning. For a transient response, the relation between the FWHM pulsewidth and the RF power is [1]

$$\tau_p \approx \sqrt{\frac{\ln 2}{M \cdot \Delta_m \cdot \pi^2 \cdot f_{\mathrm{MOD}}^2}} \propto (\Delta_m)^{-1/2} \qquad (3)$$

where M is the number of round trips counted from the start of the response. Equation (3) is only valid when the laser is within its transient response and therefore the equation is meaningless for large values of M. Now, in the case of $\Delta_f \neq 0$, i.e., in a dynamic detuning situation, energy is continuously fed to the transient response oscillations of the pulse envelope by the continued shift of the time position of the gain peak relative to the pulse peak. Hence, the laser may be thought of as having

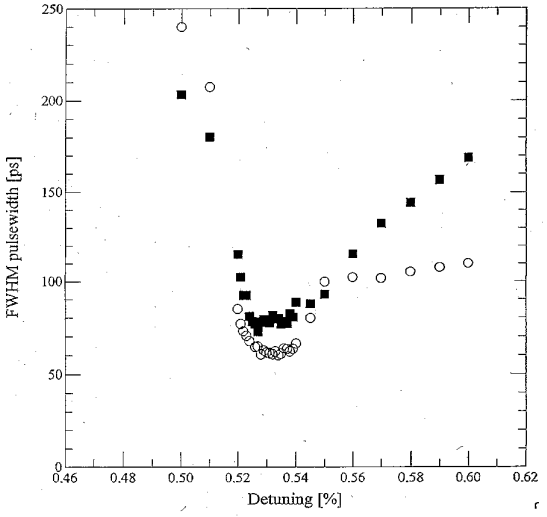

Fig. 5. Measured FWHM pulsewidth as a function of the detuning. Curves are shown for modulation at 30th (○) and 40th (■) harmonic, corresponding to 521.1 MHz and 694.8 MHz, respectively.

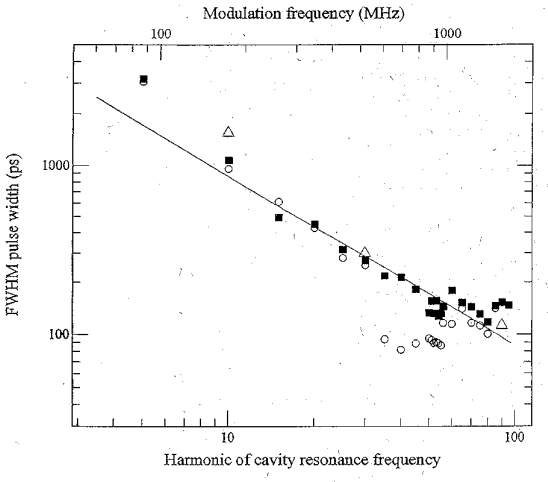

Fig. 6. Measured and simulated (△) deconvolved FWHM pulsewidth as a function of the modulation frequency. In the measurements the modulation frequency is optimized for maximum peak power in the pulses (○) and maximum average signal power (■), respectively. Shown is also a line with a slope of −1 corresponding to the dependence given by Equation (3).

an infinitely prolonged transient response and consequently, Equation (3) does in fact apply to the dynamic detuning case. Indeed, Equation (3) predicts a slope of −0.5 which is in good agreement with the measured and simulated results. We believe that the difference with respect to the absolute pulsewidth mainly is caused by the uncertainties concerning the material parameters used in our simulations.

Fig. 5 shows the deconvolved FWHM pulsewidth versus the detuning. Results are shown for SOA #1 at two different modulation frequencies. The detuning is optimized for maximum peak power in the generated pulses. Clearly, there is an optimum detuning of around $\Delta_f = 0.53\%$, a value which confirms that the ring laser operates in a dynamic detuning state. Furthermore, the optimum detuning is found to be independent of the modulation frequency. If the detuning is optimized for maximum average power in the laser signal another optimum value is found. In that case the optimum is slightly lower, i.e., around 0.50%, and the pulses have broadened significantly. This indicates that the better the mode-locking is—i.e., the higher the peak power is—the more modulation power dissipates into the nonmode-locked cavity modes causing the average power to decrease. At the point of optimum detuning the pulsewidth obtains its smallest value for the lowest modulation frequency. This is not predicted from Equation (1) and the reason is that at the lower modulation frequency double pulses evolve, i.e., pulses with two peaks. Due to a large excess carrier density caused by the low modulation frequency, the carrier depletion is not total when a pulse propagates through the SOA. Furthermore, the detuning shifts the position of the pulse peak relative to the peak of the gain modulation. Therefore, the gain is still high at the trailing edge of the pulse resulting in the evolution of a second peak. As a consequence, the presence of two or more peaks can lead to divergent results for the FWHM pulsewidth.

From Fig. 5, it is seen that a rather large detuning is needed in order to obtain optimum performance compared to most results published for linear external cavity lasers (typically, $\Delta_{f,\mathrm{optimum}} \ll 0.1\%$ [1], [13]). This indicates that the pulsewidth limitation caused by the dynamic detuning increases with increasing external cavity length.

In Fig. 6 the measured and simulated deconvolved FWHM pulsewidth versus the modulation frequency is shown. In the steady-state situation (1) predicts a $(f_{\mathrm{MOD}})^{-1/2}$ dependence for $\tau_{p,ss}$, still, better agreement is found with (3) describing the dynamic detuning state where a $(f_{\mathrm{MOD}})^{-1}$ dependence is predicted. Again a good agreement between the measurements and the simulations is obtained. These measurements also indicate that a steady-state situation as defined in [1] is never reached.

Due to the long external cavity (11.8 m) compared to linear external cavity lasers (typically, 5–15 cm) the fundamental cavity resonance frequency is relatively low, i.e. below 20 MHz. Therefore the ring laser is operated at a higher harmonic of f_{crf} in order to obtain a satisfactory pulse repetition rate. As linear external cavity lasers due to their short cavity generally are operated at first to fifth harmonic there is little published about the effect of modulating an external cavity laser at very high harmonics (e.g., at 40th to 60th harmonic). For the ring laser used in this work a pulse repetition rate of 1 GHz requires modulation at the 57th harmonic. Fig. 6 shows an optimum modulation frequency of around 800–1000 MHz when optimizing for maximum peak power in the pulses and a slight increase in pulsewidth is observed at higher modulation frequencies. When optimizing for maximum average power the optimum modulation frequency is slightly higher (i.e., around 1200 MHz) but the broadening of the pulses at high frequencies is still observed. When modulating at a high harmonic, a large number of external cavity modes do not take part in the mode-locking process. As the number of nonmode-locked cavity modes increases, the mode-locking becomes increasingly inefficient due to the higher amount of modulation power dissipated into these modes, thus resulting in broadened pulses.

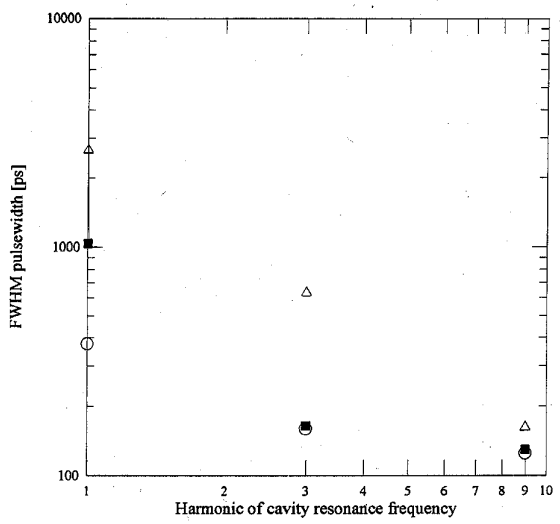

Fig. 7. Simulated FWHM pulsewidth as a function of the cavity resonance frequency harmonic. Results are shown for fiber lengths 0.5 m (○), 1.0 m (■), and 2.0 m (△).

At low modulation frequencies (<500 MHz) a significant pulse broadening is also observed. Due to an exhaustively increased excess carrier density caused by the slowly varying modulation current, the pulses turn multi peaked and broaden significantly. In extreme cases instabilities occur during numerical simulations for certain fiber lengths at these low frequencies. This is caused by the modulation frequency being comparable to the transient response of the ring laser itself, which can lead to unwanted resonance phenomena. Numerical simulations show a time constant for the transient response in the order of 2–3 ns.

In Fig. 7 the simulated FWHM pulsewidth versus the cavity resonance frequency harmonic is shown for different lengths of the external cavity. Clearly, a short external cavity is required in order to achieve short pulses which confirms that the modulation frequency should be kept high and the number of nonmode-locked cavity modes low to ensure an efficient mode-locking. The modulation frequency is different for varying fiber lengths when operating at a given harmonic but the modulation power dissipated into the nonmode-locked cavity modes is constant. Therefore the results are directly comparable. Note that the fiber lengths shown in Fig. 7 are small compared to the fiber ring used in the experiments. This has been done in order to keep computation time relatively low, i.e., below approximately 12 h. In Fig. 7, the curves show an increasing slope for longer fibers. The change in the slope from -0.50 to -1.27 when increasing the fiber length from 0.5 to 2.0 m indicates that the stability of the mode-locking decreases when long external cavities are used. Also, the curves show saturation characteristics at higher harmonics. At the ninth harmonic the length of the fiber has little significance indicating that the impact of dynamic detuning saturates for high harmonics.

Experimentally, pulses with a FWHM width of 54 ps and peak power of 2.8 mW are obtained with a time-bandwidth product of 0.7 at a repetition rate of 960.17 MHz. Numerically, pulses with a FWHM width of 59 ps, a time-bandwidth product of 0.77 and peak power of 4.5 mW are obtained at a repetition rate of 1030 MHz. The numerical result is obtained using a strongly index guided SOA structure with a spontaneous emission coupling factor $\beta = 10^{-5}$ and modulating the SOA with $\Delta_m = 1.67$.

V. Discussion and Conclusions

The SOA's used in the experiments are not optimized for use at high electrical modulation frequencies. Parasitics, impedance mismatch and structural properties thus limit the electrical modulation bandwidth to around 1.2 GHz. Doubling the modulation frequency will give a pulsewidth comparable to the result obtained by Hansen [3], but this implies the use of a SOA with an electrical modulation bandwidth of at least 2.5–3 GHz.

The difference in facet reflectivity for the two SOA's is found from simulations to be of little importance with respect to peak power and FWHM pulsewidth. The different results are therefore mainly due to differences in the semiconductor structure.

Due to the relatively low RF frequency applied to the SOA compared to the drive frequencies normally applied to mode-locked external cavity lasers, numerical simulations show a larger variation of the carrier density (peak-peak value around $8 \cdot 10^{17}\,\mathrm{cm}^{-3}$) compared to other published results, e.g., [1] ,[9]. This is simply a result of a larger number of carriers injected per period of modulation. Note, however, that the large carrier density variation does not introduce a corresponding chirp to the pulses as the predominant part of the change in carrier density takes place within the time interval where no pulse is present in the SOA.

As a consequence of the nonzero detuning, the pulse peak does not coincide with the gain peak of the carrier density modulation. This may also introduce chirp to the pulses. Often it is suggested that the lasing wavelength should be shifted below the gain peak in order to minimize chirp as such a shift leads to a decreased linewidth enhancement factor and a high differential gain. With the set up shown in Fig. 3 it is not possible, however, to tune the wavelength of the SOA ring. The wavelength is therefore entirely determined by the material gain peak of the semiconductor. One way to diminish this problem is to use multi-electrode SOA's where a gain peak tuning in the order of 5–10 nm will be possible.

In conclusions, mode-locked pulse generation with semiconductor optical amplifier (SOA) ring lasers has been investigated experimentally and numerically. The generation of 1.5 μm near transform-limited pulses with FWHM width of 54 ps, 2.8 mW peak power, and repetition rate of 960 MHz has been demonstrated experimentally. A transmission-line laser model (TLLM) has been used to simulate the generation and evolution of the mode-locked pulse train. The TLLM-model includes models of the stimulated and spontaneous emission, field attenuation, laser chirp and gain saturation due to carrier depletion. To our knowledge this is the first time the TLLM-model has been applied to a ring configuration. Simulations have shown the generation of near transform-limited pulses

with FWHM width of 59 ps, 4.5 mW peak power, and repetition rate of 1030 MHz. The pulsewidth dependence on various parameters has been investigated experimentally and numerically. The FWHM pulsewidth is found to be limited by a number of factors. Less efficient mode-locking result from (*a*) the high harmonic of the resonance frequency at which the laser is modulated and (*b*) the parasitics and impedance mismatch that limit the electrical modulation bandwidth of the SOA. This phenomenon, which is clearly seen for the ring laser, is a pulsewidth limitation that normally does not need to be taken into account for linear external cavity lasers with shorter external cavities and possible different semiconductor structure.

However, more important is the limitation imposed upon the pulsewidth by the dynamic detuning. In good agreement with the results found by Morton *et al.* [13], the results obtained in this work also indicate that dynamic detuning acts as the major limiting factor for the final pulsewidth as the results are in excellent agreement with the theory describing the dynamic detuning case. The FWHM width of the generated pulses is found to depend on the transient properties of the ring laser found for the dynamic detuning case rather than on the steady-state characteristics found for zero detuning. As stated, the impact of dynamic detuning increases for increasing length of the external cavity, which explains the relatively poor performance of the SOA ring laser compared to results obtained for mode-locked linear external cavity lasers (e.g., [1], [2], [11], [13]). A long external cavity and hence modulation at a high harmonic of the cavity resonance frequency is, however, a characteristic feature of the considered ring configuration when compared to linear cavity lasers. The fiber ring may be somewhat shortened in future experiments but for practical reasons (e.g., the fusion splicing equipment require a certain amount of fiber), one must expect a length around 5 m in total to be the lower limit in experimental setups. Little improvement of the ring laser performance can therefore be obtained by shortening the cavity.

For obtaining shorter pulses with the SOA ring laser, it is suggested that an effort should be done in order to impedance match the SOA as this is a simple method of gaining several dBs of modulation power. Furthermore, from simulations, spontaneous emission is found to have a broadening effect on the generated pulses so the SOA should be chosen as strongly index guided as possible. Also, the inherent modulation bandwidth should be high to ensure that fast modulation is possible. This implies the use of devices with a high carrier mobility and in future experiments it is therefore suggested that impedance matched SCH–MQW-structure SOA's should be used.

REFERENCES

[1] A. E. Siegman, *Lasers*. Oxford, England: Oxford University Press, 1986, pp. 336–351, 382–386, 1042–1103.

[2] A. Yariv, *Optical Electronics*. New York: Holt, Rhinehart and Winston, 1985, Appendix A, 3rd ed.

[3] P. B. Hansen, G. Raybon, M. D. Chien, U. Koren, B. I. Miller, M. G. Young, J. M. Verdiell, and C. A. Burrus, "A 1.54 μm monolithic semiconductor ring laser: CW and mode-locked operation," *IEEE Photon. Technol. Lett.*, vol. 4, pp. 411–413, 1992.

[4] P. B. Hansen, R. C. Alferness, G. Raybon, L. L. Buhl, U. Koren, B. I. Miller, M. G. Young, T. L. Koch, J. M. Verdiell, and C. A. Burrus, "Broadly tunable (202 Å) mode-locked monolithic laser with an integrated vertical coupler filter," in *13th IEEE Int. Semicond. Laser Conf.*, Sept. 1992, paper N-5, pp. 250–251.

[5] A. J. Lowery, "Transmission-line modeling of semiconductor lasers: the transmission-line laser model," *Int. J. Numer. Model.*, vol. 2, pp. 249–265, 1989.

[6] N. V. Pedersen, M.S. thesis, Tech. Univ. Denmark, 1992.

[7] A. J. Lowery, "New dynamic semiconductor laser model based on the transmission-line modeling method," *IEE Proc. J.*, vol. 134, no. 5, pp. 281–289, 1987.

[8] A. J. Lowery, N. Onodera, and R. S. Tucker, "Stability and spectral behavior of grating-controlled actively mode-locked lasers," *IEEE J. Quantum Electron.*, vol. 27, pp. 2422–2430, 1991.

[9] A. J. Lowery, "New time-domain model for active mode-locking, based on the transmission line laser model," *Proc. IEE*, vol. 136, pt. J., no. 5, 1989.

[10] M. Schell and E. Schöll, "Time-dependent simulation of a semiconductor laser amplifier: pulse compression in a ring configuration and dynamic optical bistability," *IEEE J. Quantum Electron.*, vol. 26, pp. 1005–1013, 1990.

[11] M. S. Demokan, "A model of a diode laser actively mode-locked by gain modulation", *Int. J. Electron.*, vol. 60, no. 1, pp. 67–85, 1986.

[12] J. E. Bowers, P. A. Morton, A. Mar and S. W. Corzine, "Actively mode-locked semiconductor lasers," *IEEE J. Quantum Electron.*, vol. 25, pp. 1426–1439, June 1989.

[13] P. A. Morton, R. J. Helkey and J. E. Bowers, "Dynamic detuning in actively mode-locked semiconductor lasers," *IEEE J. Quantum Electron.*, vol. 25, pp. 2621–2633, 1989.

Niels V. Pedersen, photograph and biography not available at the time of publication.

Kaj B. Jakobsen, photograph and biography not available at the time of publication.

Michael Vaa, photograph and biography not available at the time of publication.